Shah, Sahas Bikram; Osemwinyen, Osaruyi; Rasilo, Paavo; Belahcen, Anouar; Arkkio, Antero

Thermographic Measurement and Simulation of Power Losses Due to Interlaminar Contacts in Electrical Sheets

Published in:
IEEE Transactions on Instrumentation and Measurement

DOI:
10.1109/TIM.2018.2829321

Published: 01/11/2018

Document Version
Peer-reviewed accepted author manuscript, also known as Final accepted manuscript or Post-print

Please cite the original version:
Shah, S. B., Osemwinyen, O., Rasilo, P., Belahcen, A., & Arkkio, A. (2018). Thermographic Measurement and Simulation of Power Losses Due to Interlaminar Contacts in Electrical Sheets. *IEEE Transactions on Instrumentation and Measurement*, *67*(11), 2628 - 2634. https://doi.org/10.1109/TIM.2018.2829321

Thermographic Measurement and Simulation of Power Losses Due to Inter-laminar Contacts in Electrical Sheets

Sahas Bikram Shah, Osaruyi Osemwinyen, Paavo Rasilo, Anouar Belahcen, and Antero Arkkio

***Abstract*—Ferromagnetic cores of electrical machines and transformers are constructed from laminated electrical sheets to reduce eddy current losses. Burrs are formed at the edges of electrical sheets during punching and cutting. These burrs deteriorate the insulation of adjacent sheets, make inter-laminar contacts and cause inter-laminar currents to flow across the stack. It is essential to know the inter-laminar conductivity and the size of the contacts to estimate additional losses in the electrical machine. In this paper, the size of the inter-laminar contacts formed by the burrs is estimated using a novel thermographic measurement method and an analytical method. The initial temperature rise of the contacts is used in the analytical model to estimate the contact size. The electromagnetic and thermal finite element formulation validate the results obtained from analytical method. Moreover, the results obtained from measurement, analytical method and finite element method are compared. The study shows that initial temperature rise method can be used to estimate the inter-laminar contact size and electromagnetic losses if the temperature is measured immediately after energizing the sheets.**

***Index Terms*—Finite element method (FEM), hotspot, infrared (IR), infrared imaging, inter-laminar contacts, measurement and testing.**

I. Introduction

PUNCHING and cutting of electrical sheets not only deteriorate the magnetic properties of the sheets [1] but also lead to the formation of burrs at the edges of sheets [2], [3]. These sheets when pressed in an iron core form inter-laminar galvanic contacts and create short circuits between the sheets. The size of the burrs depends on the type of insulating material, insulation thickness, and age of the punching tools [4]. The electrical short circuit of the inter-laminar contacts causes excessive local heating, and in the absence of sufficient cooling, it might lead to more damage to the electrical machine [5], [6]. Therefore, it is essential to study the additional losses caused by these contacts in the electrical machine. In [7], [8], the authors have developed a surface boundary layer model to model inter-laminar contacts in electrical machines. However, the size of the burr and the conductivity of the contacts are stochastic and important parameters for the model. In this paper, the loss density due to the galvanic contacts and the burr size is estimated using a novel thermographic method.

It is well known that if a step function of heat generation is applied to a medium under steady state conditions, the instantaneous initial rate of rising of temperature at any point is directly proportional to the heat generated at the point [9]. Based on this principle, the thermal method has been exploited to obtain the core loss of electrical machines [10], [11]. It has been shown in [9] that sufficient accuracy can be obtained if measurements are made over a short period. In [9], this requirement was obtained using a chopper type dc amplifier and recorder to measure the emf generated in thermocouples. The accuracy of such measurement also depends on the type of thermocouples. Thermocouples should be thinner than the material, should not absorb the heat from the material and should be in good thermal contact to ensure fast response. In [12], an improved thermocouple made from enameled copper and constantan wires was proposed. These thermocouples were fast in response and could measure localized loss to a region of about 10 mm in diameter, and the repeatability of the measurement was within five percent [13].

Thermographic imaging techniques are widely used in various applications [14]–[16]. Nowadays, recently developed high-end thermal infrared cameras have a spatial resolution of less than 1 mm and have a time constant of less than 12 ms. Due to better spatial resolution and fast response time, thermal cameras are a better option than thermocouples. Based on the initial temperature rise method, these cameras are used in the localized measurement of iron loss in [17]–[19]. However, the estimation of the burr size with thermography method has not been studied so far.

In this paper, the size of the inter-laminar contacts formed by the burrs is studied using thermographic measurement, analytical method and electromagnetic and thermal finite element formulation. First, a short circuit measurement is performed to obtain the short circuit current and electric potential between the sheets. The initial temperature rise of the hotspot formed by inter-laminar contact is also measured using a thermal camera and used in analytical calculation to estimate the size. Later, the estimated size is studied in the electromagnetic and thermal finite element method using the measured electric potential in detail and obtained results from the simulations and measurement are compared. The temperature gradient predicted by electromagnetic-thermal finite element simulations gave a good agreement to the measurement at higher supplied current.

Manuscript received October 9, 2017; revised XX-XX-XXXX. Corresponding author: S. B. Shah (email: sahas.bikram.shah@aalto.fi).

S.B. Shah, O. Osemwinyen, A. Belahcen and A. Arkkio are with Department of Electrical Engineering and Automation, Aalto University, Espoo, Finland.

P. Rasilo is with Laboratory of Electrical Energy Engineering, Tampere University of Technology, Finland

II. Measurement

A. Measurement setup

The 0.5 mm non-oriented electrical sheet as shown in Fig. 1 is used for the experimental study.

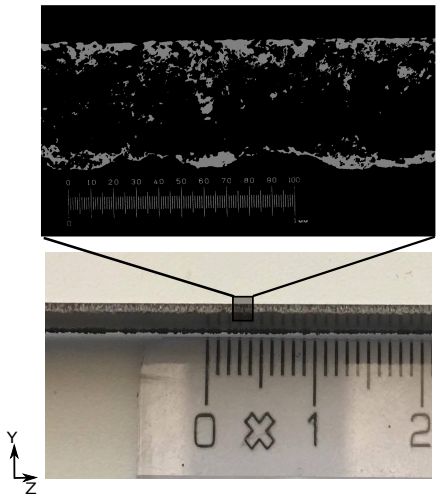

Fig. 1. Illustration of the burrs at the edges of the electrical sheet

The material grade of the sheet is M270-50A and it is semi-processed. The insulation of upper surfaces of the sheets are removed to supply the power. However, the surfaces between the sheets are insulated. The image is taken using the magnifying camera IMPERX GEV-B1922C-SC000 along with a calibration scale. 1 pixel is equivalent to 0.01 mm. Two electrical sheets are placed in such a way that only one edge is not insulated. A thin insulation layer of 0.1 mm is placed between the sheets to ensure the galvanic contacts to be present at only one edge. The sheets are then energized with DC supply, and the initial temperature rise is recorded using the thermal camera. The measurement setup is designed to perform the short circuit and thermal test of the electrical sheet. It consists of a rotating measuring unit and a force sensor to measure the applied force. The rotational feature of the measuring unit allows capturing thermal image from all sides of the electrical sheets. The repeatability of the measurement is ensured by measuring the voltage and current at the same applied force and taking the average of three measured values. The applied force is 4237 N. Each measurement is repeated for three times, and the average value is considered. The voltage measuring block consists of needle probes attached to a spring both at the bottom and top of the sample. The sheets are then energized with DC supply using two copper plates and placing electrical sheets in between them. There are three needle probes each of diameter 0.1 mm. One of the probes is used to supply the voltage which is connected to cooper plates and other two measure the electric potential over the galvanic contacts. DWE-50-PCI32 data acquisition system is used to acquire the voltage and current at the rate of 100 kHz. A switch is connected in series with the power supply and is synchronized with the thermal IR camera recording. The short circuit measurement setup is shown in Fig. 2.

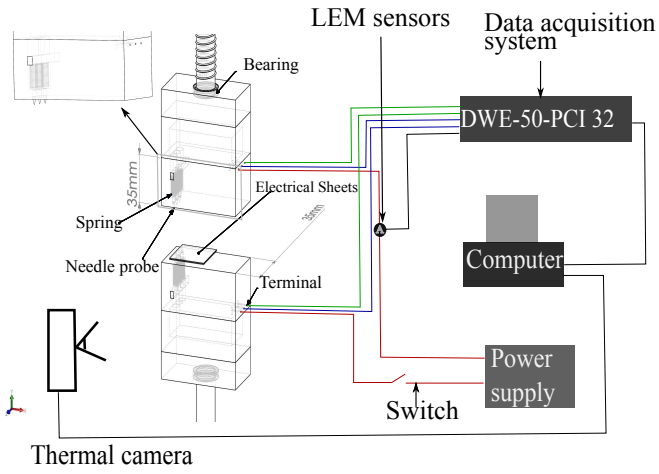

Fig. 2. A schematic of shortcircuit measurement setup

B. Shortcircuit measurement

The short circuit current and voltage are measured immediately after closing the switch. The short circuit currents measured are given by i_{s1}, i_{s2}, i_{s3}, and i_{s4}. It is important to remember here that the resistance of the hotspot or burr is stochastic. Due to significant burrs at the edge of the sheets which are visible in Fig. 1, there is a constant galvanic contact along one side of the edge of the sheets. However, the width of the burr inwards from the edge of the electrical sheets is an unknown quantity. The width of the burr is estimated from thermal measurement and analytical calculation. The estimated burr width is studied in detail with an electromagnetic finite element formulation.

C. Thermal measurement

The thermal measurement was done using FLIR T640 thermal camera. The specification of the thermal camera is shown in Table I.

TABLE I
FLIR T640 THERMAL CAMERA SPECIFICATION

Frame rate	30 Hz
Temperature range	233.15 K to 2273 K
Accuracy	$\pm$ 2% of reading
Field of view	32 $\times$ 24 mm (close up lens)
Detector type	uncooled microbolometer (640 $\times$ 480 pixel)

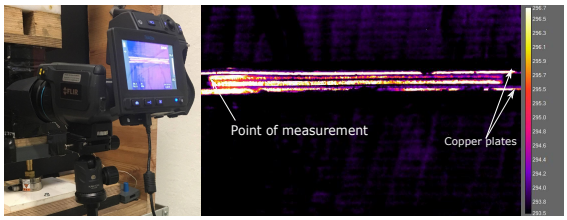

Fig. 3. Measured temperature distribution and point of measurement at a hot spot

The temperature distribution obtained from the thermal camera is shown in Fig. 3.

III. Computation Method

A. Analytical method

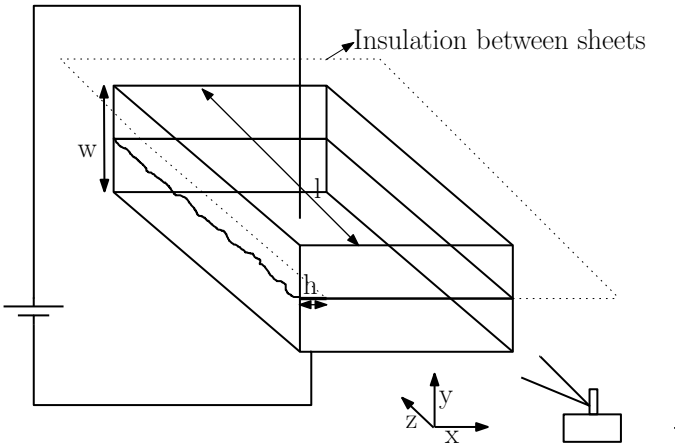

Fig. 4. Illustration of two electrical sheets, insulation layer and thermal camera

Two electrical sheets as shown in Fig. 4 are considered, where l and h are the length and burr width of the studied electrical sheets, respectively. w is the total thickness of the stack of two sheets and the insulating layer between them. Based on the initial temperature rise method, if the temperature is measured immediately after energizing the sheets, the loss density in (W/m^3) can be written as

$$\rho C_p \left(\frac{\partial T}{\partial t}\right)_{\mathrm{m}} = \frac{VI}{lhw}, \tag{1}$$

where, V and I are the measured voltage over the contact and short circuit current, respectively. ρ, C_p, T and t are the density, specific heat capacity of the material, temperature and time, respectively. $\left(\frac{\partial T}{\partial t}\right)_{\mathrm{m}}$ is the average temperature rise obtained from the measurement at a point of the conducting edge. The measured temperature rise is shown in Fig. 5.

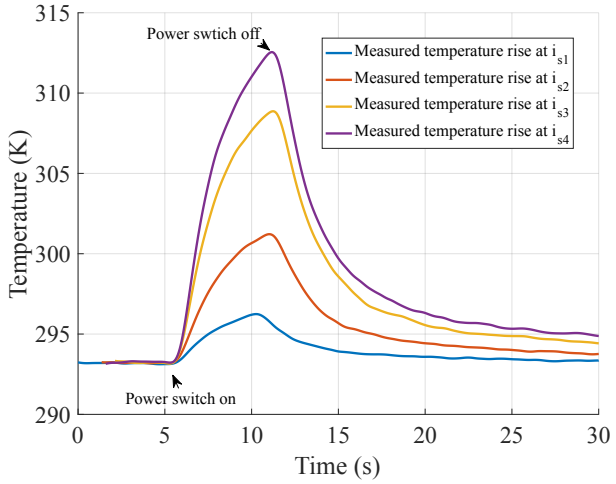

Fig. 5. Measured temperature at the hotspot at different current readings.

Then, the average of temperature gradient of temperature is taken between turn-on and turn-off time. From the measured values of voltage, short circuit current and average temperature rise, an expression can be obtained as

$$\zeta_j = \rho C_p h = \frac{VI}{wl\left(\frac{\partial T}{\partial t}\right)_{\mathrm{m}_j}}. \tag{2}$$

Similarly, the loss density of the contact can also be written as

$$\frac{J^2}{\sigma} = \rho C_p \left(\frac{\partial T}{\partial t}\right)_{\mathrm{m}}, \tag{3}$$

$$\frac{I^2}{l^2 h\sigma} = \zeta \left(\frac{\partial T}{\partial t}\right)_{\mathrm{m}}, \tag{4}$$

where, $J = \frac{I}{lh}$ is the current density. The expression of product of conductivity and burr width can be obtained by substituting (2) in (4). $\left(\frac{\partial T}{\partial t}\right)_{\mathrm{m}}$ are measured at four short-circuit current levels. The average product of conductivity and burr width can be estimated by taking the average of measured values at different current levels as given by

$$\overline{\sigma h} = \frac{1}{n}\sum_{j=1}^{n} \frac{I_j^2}{l^2 \zeta_j \left(\frac{\partial T}{\partial t}\right)_{\mathrm{m}_j}}, \tag{5}$$

where n is the number of measurements and $\overline{\sigma h}$ is the average of product of conductivity and burr width. The resistivity temperature coefficient of the considered NO electrical sheet is 0.006/K. The maximum temperature difference is 18 K as can be seen in Fig. 5. In burr width calculation (5), the temperature rise was taken into consideration.

B. Electromagnetic and thermal finite element formulation

The potential distribution around the contact between the two sheets is modeled by 2D FEM formulation. Due to symmetry only one of the two sheets is considered as shown in Fig. 9. The differential form of Faraday's law in the absence of time varying magnetic flux density is given by

$$\nabla \times \mathbf{E} = 0, \tag{6}$$

where $\mathbf{E}$ is the electric field and can be written in terms of electric potential V as

$$\mathbf{E} = -\nabla V. \tag{7}$$

When a DC voltage is connected to the sheets, a steady current flows through the sheets and inter-laminar contacts. The continuity equation is given by

$$\nabla \cdot \mathbf{J} = 0. \tag{8}$$

The current density is given by

$$\mathbf{J} = \sigma \mathbf{E}, \tag{9}$$

where, σ is the conductivity of the sheets. Using (8) and (9), the following equation is obtained:

$$-\sigma \nabla^2 V = 0. \tag{10}$$

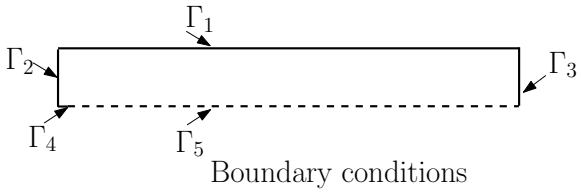

Fig. 6. A boundary conditions for the electromagnetic formulation

The boundary Γ of the sheet is divided into five parts as shown in Fig. 6 on which the following boundary conditions are assumed:

$$\begin{aligned} V &= 0 \text{ on } \Gamma_4 \\ V &= \begin{cases} V_{\text{on}}, & \text{on } \Gamma_1 \text{ if } t_{\text{on}} \leq t < t_{\text{off}} \\ V_{\text{off}}, & \text{on } \Gamma_1 \text{ if } t < t_{\text{on}} \text{ or } t \geq t_{\text{off}} \end{cases} \\ \frac{\partial V}{\partial n} &= 0 \text{ on } \Gamma_2, \Gamma_3, \Gamma_5, \end{aligned} \tag{11}$$

where t_{on} and t_{off} are the time instants when power is turned on and off, respectively. V_{on} and V_{off} are potentials measured at those instants. Equation (10) is then solved using the finite element method with 5356 second order triangular elements. The solution of V is shown in Fig. 9. The resistive loss density in (W/m^3) is computed from

$$p_{\text{Fe}} = \mathbf{E} \cdot \mathbf{J}, \tag{12}$$

In [17], the initial temperature rise method is used in calculating iron loss based on the constant ambient temperature assumptions. In [19] temperature was measured inside the vacuum chamber. The constant ambient temperature means that there is no heat diffusion, i.e., $\nabla T = 0$. In this paper, heat equation and the electromagnetic formulation are solved together. First, the resistive loss is calculated from the electromagnetic formulation and coupled to the heat equation as the heat source. The heat equation is given by

$$\rho C_p \frac{\partial T}{\partial t} + \nabla \cdot \mathbf{q} = p_{\text{Fe}} \tag{13}$$

$$\mathbf{q} = -k \nabla T \tag{14}$$

where, ρ, C_p, k, p_{Fe}, and $\mathbf{q}$ are the density, specific heat capacity, thermal conductivity, heat source, and heat flux, respectively. The heat transmitting to the surroundings is given by

$$\mathbf{n} \cdot \mathbf{q} = h_{\text{ext}} \left(T - T_{\text{ext}} \right). \tag{15}$$

where, T_{ext} is the sorrounding temperature and h_{ext} is the convective heat constant. This additional conditions was applied to the boundaries of the geometry. The parameters for thermal simulations for the M270-50A electrical steel are listed in Table II.

IV. Results and Discussion

The electromagnetic and thermal finite element formulations were implemented using the estimated burr width. The average $\overline{\sigma h}$ was obtained as 27.3 S from the analytical equation (5). These inter-laminar contacts are random. However, based on the assumptions of constant galvanic contacts along the z direction as shown in Fig. 1 and Fig. 4, the estimated burr width from the analytical calculation was 0.0135 mm using the conductivity from Table II and taking temperature rise into account.

TABLE II
Parameters for the simulation of non oriented electrical sheets [20], [21]

Density [kg/m^3]	7600
Convective heat constant [W/m^{2}K]	12
Thermal conductivity [W/mK]	30
Electrical conductivity [S/m]	1.8 $\times 10^6$
Specific heat capacity [J/kgK]	461

TABLE III
Measured and simulated short circuit currents

	Measured [A]	**Simulated [A]**	**Percentage difference** [%]
i_{s1}	1.93	1.83	4.91
i_{s2}	4.27	4.09	4.14
i_{s3}	7.04	6.92	1.71
i_{s4}	8.46	8.47	0.17

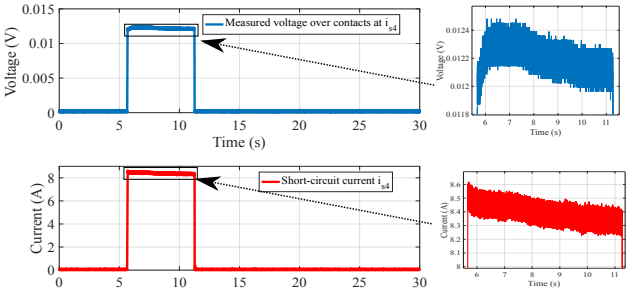

Fig. 7. The voltage and short circuit current waveforms

TABLE IV
Measured and simulated temperature gradients

	Measured $\left(\frac{\partial T}{\partial t}\right)_{\mathbf{m}}$ **[K/s]**	**Simulated** $\left(\frac{\partial T}{\partial t}\right)_{\mathbf{s}}$ **[K/s]**	**Percentage difference** [%]
i_{s1}	0.88	0.61	30.6
i_{s2}	2.25	2.2	2.2
i_{s3}	4.59	4.50	1.9
i_{s4}	6.70	6.76	0.9

The short circuit currents obtained from measurement and simulations are listed in Table III. The voltage and shortcircuit current waveform is shown in Fig. 7. The average value of voltage and shortcircuit current between turn on and turn off time are considered. In Table IV, the temperature gradient measured with the thermal camera and the temperature gradient obtained from finite element method are tabulated. At

low current i_{s1}, the temperature rise is less than two degrees Kelvin, so this results in large differences. The losses at current i_{s2}, is about five times compared to losses at i_{s1}. The temperature rise at i_{s2} is also about three times compared to i_{s1}. Hence, this results in small differences between measured and simulated results. Moreover, at higher currents, the agreement in Table IV is very good. Hence, the short circuit current (i_{s4}) and the electric potential related to this measurement was used for further FEM simulations. The loss density calculated with electromagnetic and thermal finite element method at current level of i_{s4} is shown in Fig. 8. Thermal loss density at the hotspot is calculated using the formula $\rho C_p \left(\frac{\partial T}{\partial t}\right)_s$. $\left(\frac{\partial T}{\partial t}\right)_s$ is the average of temperature gradient obtained between turn on and turn off time using the thermal finite element simulations. It can be seen from Fig. 8 that the average loss density from the thermal calculation is equivalent to electromagnetic calculation only for few seconds after energizing the sheets. Hence, to estimate the loss density from the thermal measurement, it is essential to measure the initial temperature rise immediately after the sheets are energized. In this paper, with the use of

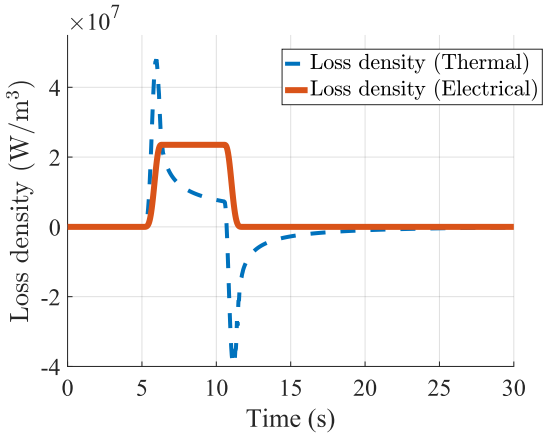

Fig. 8. A comparison of loss density calculated from thermal and electrical simulations

thermal camera, it was possible to record the temperature rise of the contacts for 30 seconds with the time resolution of 30 ms. The electric potential distribution and current density distribution calculated from the solution of the electromagnetic FE model are shown in Fig. 9 and Fig. 10, respectively. The temperature distribution obtained by solving the heat equation and the discretized mesh is shown in Fig. 11. The temperature profile of contacts from measurement and simulation considering the estimated burr width is shown in Fig. 12. It can be seen that the temperature profile behaves similarly after energizing the sheet but after turning off the power, there is a significant difference in the temperature behavior which is mainly because of the atmospheric condition and convective constant. However, in this paper, we are mainly interested in the initial rise of the temperature which shows the similar trend after switching on the power. The rate of temperature rise was calculated taking the average between turn on and turn off time as shown in Fig. 12. The proposed simulation and measurement system is applicable even with a stack provided the size of stack is within the scope of the thermal camera lens.

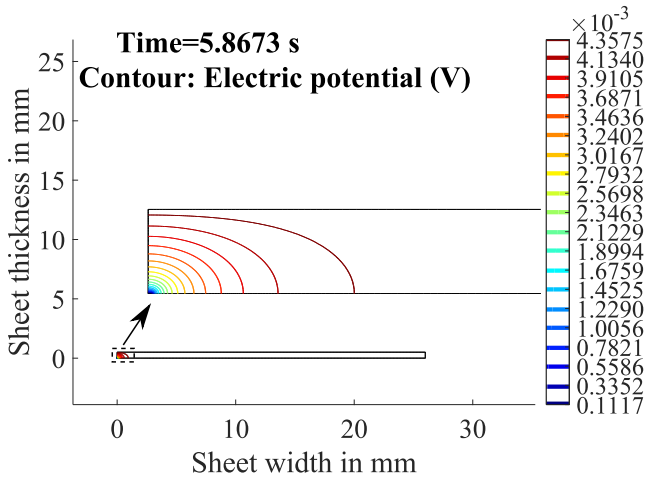

Fig. 9. A solution of electric potential at a hot spot

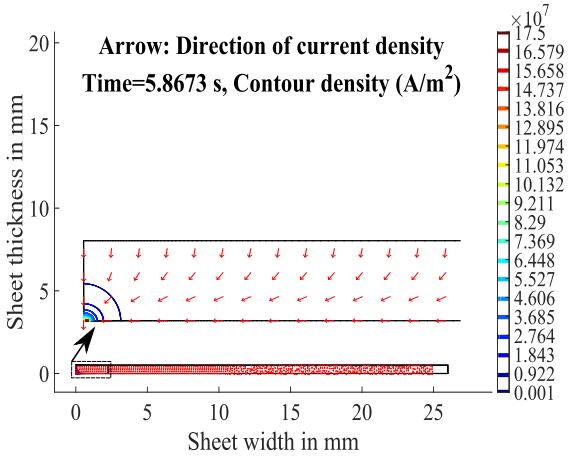

Fig. 10. A contour of current density at a hot spot

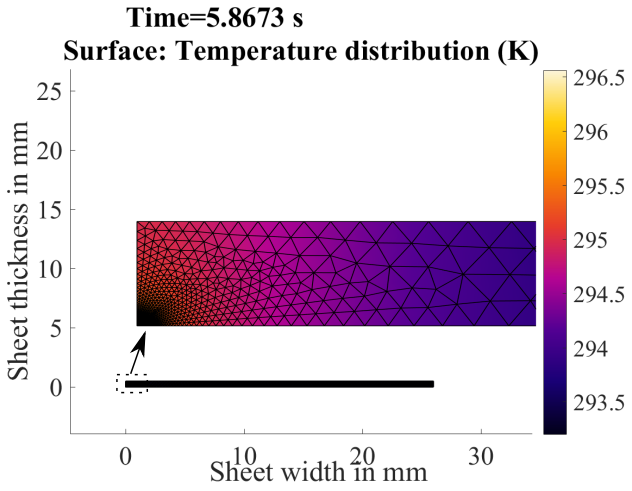

Fig. 11. Simulated temperature at a hot spot

Probably in a stack, the contacts are not uniform, and multiple hot spots are present. Therefore, multiple measurement points are needed to measure initial rate of temperature.

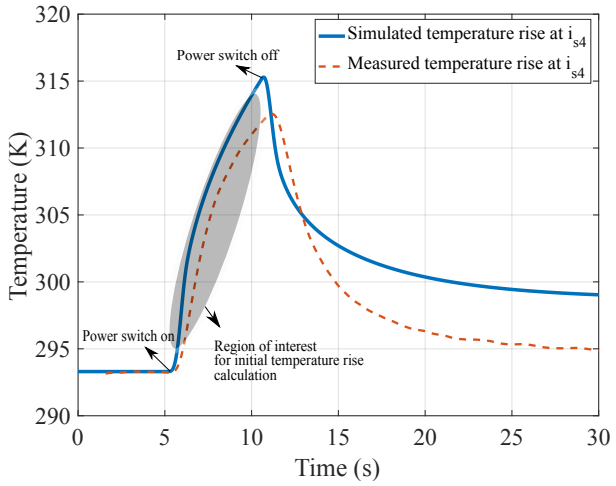

Fig. 12. Simulated and measured temperature at a hot spot

V. Conclusion

Burrs are formed at the edges of electrical sheets during punching and cutting. In this paper, the burr width size is estimated using a novel thermographic method. This paper studies and validates the initial temperature rise method to calculate the electromagnetic losses. At supply currents higher than 4 A, the temperature gradient predicted by electromagnetic-thermal finite element simulations gave a good correspondence to that measured by averaging over the turn on and turn off time. The smaller the time constant of the measurement device, the better will be the accuracy. This method was implemented, and the burr width size of the electrical sheet was estimated. Even though h is small, it represents the conducting width of the conducting layer in insulated electrical sheets and creates hot spots increasing the temperature of the machine. In [7] authors have developed a surface boundary layer model to account for interlaminar contacts that occur between the electrical sheets in electrical machines. The surface boundary layer formulation is based on magnetic vector potential formulation and finite element method. It adds the contribution of product of conductivity and burr width at the edges of stator of electrical machines. However, these interlaminar contacts are random in nature and for the estimation of additional losses in electrical machines the quantification of $\overline{\sigma h}$ is essential. The method developed in this paper along with the previous methods allows us to calculate the maximum temperature rise of the electrical machines during inter-laminar short circuit.

Acknowledgment

The research leading to these results has received funding from the European Research Council under the European Unions Seventh Framework Programme (FP7/2007-2013) ERC grant agreement no 339380. P. Rasilo acknowledges the Academy of Finland for financial support.

References

[1] A. Kedous-Lebouc, B. Cornut, J. Perrier, P. Manf, and T. Chevalier, "Punching influence on magnetic properties of the stator teeth of an induction motor," *Journal of Magnetism and Magnetic Materials*, vol. 254255, pp. 124 – 126, 2003, proceedings of the 15th International Conference on Soft Magnetic Materials (SMM15).

[2] A. C. Beiler and P. L. Schmidt, "Interlaminar eddy current loss in laminated cores," *Transactions of the American Institute of Electrical Engineers*, vol. 66, no. 1, pp. 872–878, Jan 1947.

[3] L. V. Bewley and H. Poritsky, "Intersheet eddy-current loss in laminated cores," *Electrical Engineering*, vol. 56, no. 3, pp. 344–346, March 1937.

[4] H. Wang and Y. Zhang, "Modeling of eddy-current losses of welded laminated electrical steels," *IEEE Transactions on Industrial Electronics*, vol. 64, no. 4, pp. 2992–3000, April 2017.

[5] G. B. Kliman, S. B. Lee, M. R. Shah, R. M. Lusted, and N. K. Nair, "A new method for synchronous generator core quality evaluation," *IEEE Transactions on Energy Conversion*, vol. 19, no. 3, pp. 576–582, Sept 2004.

[6] Z. Posedel, "Inspection of stator cores in large machines with a low yoke induction method-measurement and analysis of interlamination short-circuits," *IEEE Transactions on Energy Conversion*, vol. 16, no. 1, pp. 81–86, Mar 2001.

[7] S. B. Shah, P. Rasilo, A. Belahcen, and A. Arkkio, "Estimation of additional losses due to random contacts at the edges of stator of an electrical machine," *COMPEL - The international journal for computation and mathematics in electrical and electronic engineering*, vol. 34, no. 5, pp. 1501–1510, 2015. [Online]. Available: http://dx.doi.org/10.1108/COMPEL-02-2015-0083

[8] S. B. Shah, P. Rasilo, H. Hakula, and A. Arkkio, "Efficient finite element method to estimate eddy current loss due to random interlaminar contacts in electrical sheets," *International Journal of Numerical Modelling: Electronic Networks, Devices and Fields*, 2017.

[9] A. J. Gilbert, "A method of measuring loss distribution in electrical machines," *Proceedings of the IEE - Part A: Power Engineering*, vol. 108, no. 39, pp. 239–244, June 1961.

[10] A. Moses, B. Thomas, and J. Thompson, "Power loss and flux density distributions in the t-joint of a three phase transformer core," *IEEE Transactions on Magnetics*, vol. 8, no. 4, pp. 785–790, Dec 1972.

[11] C. M. Laffoon and J. F. Calvert, "Abridgment of additional losses of synchronous machines," *Journal of the A.I.E.E.*, vol. 46, no. 6, pp. 573–582, June 1927.

[12] D. A. Ball and H. O. Lorch, "An improved thermometric method of measuring local power dissipation," *Journal of Scientific Instruments*, vol. 42, no. 2, p. 90, 1965. [Online]. Available: http://stacks.iop.org/0950-7671/42/i=2/a=307

[13] G. Radley and A. Moses, "Apparatus for experimental simulation of magnetic flux and power loss distribution in a turbogenerator stator core," *IEEE Transactions on Magnetics*, vol. 17, no. 3, pp. 1311–1316, May 1981.

[14] D.-H. Lee, "Thermal analysis of integrated-circuit chips using thermographic imaging techniques," *IEEE Transactions on Instrumentation and Measurement*, vol. 43, no. 6, pp. 824–829, Dec 1994.

[15] T. E. Salem, D. Ibitayo, and B. R. Geil, "Validation of infrared camera thermal measurements on high-voltage power electronic components," *IEEE Transactions on Instrumentation and Measurement*, vol. 56, no. 5, pp. 1973–1978, Oct 2007.

[16] F. Attivissimo, A. D. Nisio, C. G. C. Carducci, and M. Spadavecchia, "Fast thermal characterization of thermoelectric modules using infrared camera," *IEEE Transactions on Instrumentation and Measurement*, vol. 66, no. 2, pp. 305–314, Feb 2017.

[17] H. Hamzehbahmani, A. J. Moses, and F. J. Anayi, "Opportunities and precautions in measurement of power loss in electrical steel laminations using the initial rate of rise of temperature method," *IEEE Transactions on Magnetics*, vol. 49, no. 3, pp. 1264–1273, March 2013.

[18] L. Ferraris, F. Franchini, and E. Pošković, "A thermographic method for the evaluation of the iron losses distribution in electromagnetic devices," in *IECON 2016 - 42nd Annual Conference of the IEEE Industrial Electronics Society*, Oct 2016, pp. 1584–1589.

[19] H. Shimoji, T. Todaka, and M. Enokizono, "Core loss distribution measurement of electrical steel sheets using a thermographic camera," *Przeglad Elektrotechniczny (Electrical Review)*, vol. 87, no. 9b, pp. 65–69, 2011.

[20] J. Pyrhönen, T. Jokinen, and V. Hrabovcová, *Design of Rotating Electrical Machines*. UK: John Wiley & Sons, Ltd, 2013, ch. Losses and Heat Transfer, pp. 523–569. [Online]. Available: http://dx.doi.org/10.1002/9781118701591.ch9

[21] SIR-Gruppen, "Electrical steel non oriented fully processed," Cogent Power Ltd, Tech. Rep., 2002.